Numerical Calculation of Turbulent Flow and Combustion in an Otto Engine Using the Eddy Dissipation Concept

B.Grimsmo and B.F.Magnussen

Division of Thermodynamics
The Norwegian Institute of Technology
N-7034 Trondheim-NTH
Norway

ABSTRACT

The Eddy Dissipation Concept of Magnussen is applied to predict the turbulent combustion in an Otto engine. The newest version of this concept is described. This version is basically the same as the earlier model, only a minor change in the description of mass fraction of fine structure being able to react now gives a slightly steeper turbulent flame front and a faster burning.

The k-ε-model used is extended with two additional terms which include compression/-expansion effects due to piston movement and flame expansion and effects caused by pressure density interaction generated by the flame.

Calculations have been done for the complete four stroke cycle of a two dimensional axis symmetrical simple flat headed pancake piston engine. The geometry has been selected for reasons of simplicity and saving computer time, addressing the main efforts to the treatment and understanding of the modelling of the non resolvable physical processes of the complex flow and combustion during the four strokes of the Otto engine cycle. The results obtained show good agreement with experimental data found in the literature.

The present paper demonstrates and discusses the applicability of the EDC concept for calculations of combustion in engines. It also discusses the application of the extended k-ε-model and demonstrates its effect on the combustion. The paper also give some comments on general topics connected to the treatment and basic understanding of engine turbulence in numerical calculation.

1 Introduction

The combustion process is the key to both the fuel consumption and the emission of pollutants in piston engines. The engine industry is interested in and intend improving the efficiency of engine combustion to develop engines which run with higher compression and leaner mixtures. Unfortunately physical barriers like knock and lessened burning speed restrain these intentions. The solution of both problems is possibly to speed up the reaction rate by increasing the turbulent mixing.

In the literature [1-9], various combustion models have been applied when numerical simulations of the combustion process in piston engines have been performed. One of these models has been the Eddy Dissipation Concept, EDC [10].

This model has shown great generality being able to predict diffusion flames, premixed flames and explosions without the need of changing constants. It is especially attractive since it has a close and clear connection to the classical turbulence energy transfer theory and also because of its simple way of application and its low need for computer resources.

From the earlier works seen in the literature, it is not always clear whether this method has been used correctly or not.

It has been a motive of this work not to adjust model constants in order to get the best fitted results, but to use all models as they are to test their performance and uncover their weaknesses.

2 Physical Models

The density weighted time averaged compressible Reynolds equations, suitably extended to include chemical reactions in a mixed material and spatial description, are solved. In spatial description these equations have the typical form

$$\frac{\partial}{\partial t}(\bar{\varrho}\tilde{\varphi}) + \frac{\partial}{\partial x_j}(\bar{\varrho}\tilde{\varphi}\tilde{u}_j + \overline{\varrho\varphi''u_j''}) - \frac{\partial}{\partial x_j}\overline{\Gamma_\varphi \frac{\partial}{\partial x_j}\varphi} + \bar{\varrho}\tilde{S}_\varphi = 0 \qquad (1)$$

The ensemble mass weighted mean and the related fluctuation of repeated experiments are defined by respectively

$$\tilde{u}(t) = \frac{1}{\bar{\varrho}(t)}\frac{1}{N}\sum_{i=1}^{i=N}\varrho(t)u(t) \qquad (2)$$

and

$$u''(t) = \tilde{u}(t) - u(t) \qquad (3)$$

By neglecting fluctuating density correlations in the conventional averaged equations, these equations become similar to the density weighted form except for that over bars are replaced tildes and primes by double primes. This means that solving conventional averaged equations neglecting the density fluctuation terms is actually the same as solving the density weighted form shutting one's eyes to the difference of the treated values.

The conservation equations solved are the equations of mass, momentum, internal energy, mass fractions of species, and turbulence parameters, all together ten equations in two space dimensions. The turbulence diffusivity, and the reactants to products conversion rate are modeled.

2.1 Turbulence model

An extended version [11] of the k-ε model [12] is used which includes the effects of compression (expansion) of the flow on turbulence properties.

The compression effects are accounted for by assuming that the total angular momentum of the turbulence vortices is conserved during the changes of the volume of the fluid due to movement of the piston and expansion of gases in the combustion process. The method is based on the rapid distortion theory with the assumption that the angular momentum of different eddies is redistributed very fast by the interactions between the eddies and then is isentropic.

The influence of the interaction between pressure and density is accounted for by modelling the $u''\partial p/\partial x$ term in the exact form of the k-equation.

The turbulence diffusion term in the momentum equation is expressed by

$$\overline{-\varrho u_i'' u_j''} = \mu_t\left(\frac{\partial \tilde{u}_i}{\partial x_j} + \frac{\partial \tilde{u}_j}{\partial x_i}\right) - \frac{2}{3}\delta_{ij}\left(\bar{\varrho}k + \mu_t \frac{\partial \tilde{u}_l}{\partial x_l}\right) \qquad (4)$$

and the turbulent diffusion terms in the equations for scalar properties are expressed by

$$\overline{-\varrho\varphi'' u_j''} = \frac{\partial}{\partial x_j}\frac{\mu_t}{\sigma_{t,\varphi}}\frac{\partial}{\partial x_j}\tilde{\varphi} \qquad (5)$$

where

$$\mu_t = \bar{\varrho} C_d \frac{k}{\varepsilon^2} \qquad (6)$$

The source terms of the model equations for k and ε are

$$S_k = P_k - \bar{\varrho}\varepsilon \qquad (7)$$

and

$$S_\varepsilon = C_1\frac{\varepsilon}{k}P_k - C_2\bar{\varrho}\frac{\varepsilon^2}{k} + C_3\bar{\varrho}\varepsilon\frac{\partial \tilde{u}_l}{\partial x_l} \qquad (8)$$

P_k represents the production of turbulence kinetic energy and is modeled by

$$P_k = \overline{-\varrho u_i'' u_l''}\frac{\partial \tilde{u}_l}{\partial x_j} = \mu_t G_k - \frac{2}{3}\frac{\partial \tilde{u}_l}{\partial x_l}\left(\bar{\varrho}k + \mu_t\frac{\partial \tilde{u}_l}{\partial x_l}\right) - \frac{1}{\bar{\varrho}^2}\frac{\mu_t}{\sigma_t}\frac{\partial \bar{\varrho}}{\partial x_l}\frac{\partial \bar{p}}{\partial x_l} \qquad (9)$$

where the last term is the modeled pressure/density effect term. All the terms with a divergence expression in the above equations represent dilatation effects.

G_k is expressed by

$$G_k = \frac{\partial \tilde{u}_l}{\partial x_j}\left(\frac{\partial \tilde{u}_l}{\partial u_j} + \frac{\partial \tilde{u}_j}{\partial x_l}\right) \qquad (10)$$

It should be noted that in experimental investigations an averaging procedure like the is based on the ensemble average over a number of nonreproducible experimental engine cycles, does not separate cycle-to-cycle variation of the mean flow from the turbulence fluctuations. Therefore a measured turbulence intensity is necessarily overestimated.

In the calculations, it is easy to imagine the turbulence fluctuations divided from the mean flow. Numerically the mean flow is reproducible and the definition of ensemble average is fulfilled. Hence, calculations have no counterpart to the measured overestimation of turbulence, and the calculated values should for this reason be treated as in-cycle values. Turbulence properties respond to the mean velocity field of the individual cycle in which the eddy viscosity represents a factor of the current lateral fluxing. Trying to treat phase averaged values in the calculations using flux models like the k-ε-model, and hence including cycle-to-cycle effects in the eddy viscosity, will cause an inclusion of nonexisting mixing.

The effects of the walls inside the engine cylinder is poorly understood. In the present work, the turbulent quantities in the wall cells is calculated from the transport equations similar to how it is done in the general cells, applying a no transport restriction on the wall surface (w)

$$\left(\frac{\partial k}{\partial y}\right)_w = 0\,, \qquad \left(\frac{\partial \varepsilon}{\partial y}\right)_w = 0 \qquad (11,12)$$

To ensure a proper length scale limitation and turbulence damping near the wall (nw), the dissipation ε in the wall cells is controlled by the following procedure

$$\text{if } l_{nw} > y_{nw} \quad \text{then} \quad \varepsilon_{nw} = \frac{C_d \, k_{nw}^{3/2}}{y_{nw}} \tag{13}$$

$$\text{if } l_{nw} < y_{nw} \quad \text{then} \quad \varepsilon_{nw} = \frac{C_d \, k_{nw}^{3/2}}{l_{nw}} \tag{14}$$

$$\text{where} \quad l_{nw} = \frac{C_d \, k_{nw}^{3/2}}{\varepsilon_{nw}} \tag{15}$$

The necessity of this control is obvious since the two last terms of the ε-equation exhibit a singular nature because of k's tendency to approaching zero at low velocities near the wall, see Eqs. (7,8).

The parameters of the flow trough an open valve is prescribed according to the estimates of Gosman et al.[13]

The heat loss to the walls is affecting the combustion through the turbulence by producing a high density/low temperature layer. This layer does not only affect the combustion through the turbulence, but the low temperature also reduces the reaction rate, and under certain circumstances it might also cause extinction. Furthermore, the quenchlayer is expected to reduce the expansion effects.

The mechanisms behind the heat loss to the piston head and cylinder walls are also poorly understood. In the calculations this heat loss is accounted for by adding an extra source term in the near wall cells, given by

$$q_w = \frac{\mu_t C_v}{\sigma_{t,i}} \frac{(T_{nw}-T_w)}{y_{nw}} \tag{16}$$

This at least ensure that the heat loss takes place where and when this process is expected to go on, and the main effects of gas expansion are included. The total fraction of heat loss to the walls during a complete cycle modeled by this method has shown to be of the same magnitude as for real engines.

The near wall effective viscosity is given by Eq. (6) applying k_{nw} and ε_{nw}.

The constants used are

$C_d = 0.09$, $C_1 = 1.44$, $C_2 = 1.92$,

C_3 = varied, $\sigma_{t,k} = 1.0$, $\sigma_{t,\varepsilon} = 1.3$,

$\sigma_{t,i} = 0.7$ $C_4 = 1/\sigma_t$ = varied

2.2 Combustion Model

The fast chemistry assumption is assumed, and the fuel in the gas phase is assumed to react irreversibly with the available oxygen, via a single step reaction, to produce products according to the following scheme

$$\text{Fuel} + r_{fu} \text{ oxygen} \rightarrow (1+r_{fu}) \text{ products} \tag{17}$$

where r_{fu} is the stoichiometric oxygen requirement of the fuel. The formation rates appearing in the conservation equations for mass fraction of species are expressed by

$$\bar{\varrho}\tilde{\omega}_{fuel} = R_{fuel}$$

$$= \text{model}(\tilde{Y}_{fuel}, \tilde{Y}_{O_2}, \tilde{Y}_{prod}, \text{parameters}) \tag{18}$$

$$R_{O_2} = r_{fu} R_{fuel} \tag{19}$$

and

$$R_{prod} = (1+r_{fu}) R_{fuel} \tag{20}$$

while the source term of the internal energy equation is expressed by

$$\bar{\varrho}\tilde{S}_i = R_{fuel} \cdot \Delta E \tag{21}$$

The Eddy Dissipation Concept by Magnussen[10] is used to predict the fuel to products conversion rate. This model is based on the fact that the molecular mixing between the reactants is closely connected to the dissipation of turbulent kinetic energy and takes place in the isolated regions where fine structures are located.

The scales of the fine structures are closely related to the Kolmogorov scales and are expressed by

$$u^* = 1.74 \, (\varepsilon\nu)^{1/4} \tag{22}$$

$$L^* = 1.43 \, \nu^{3/4}/\varepsilon^{1/4} \tag{23}$$

The mass fraction occupied by the fine structures and the mass fraction occupied by fine structure regions are given respectively by

$$\gamma^* = 9.7 \left(\frac{\nu\varepsilon}{k^2}\right)^{3/4} \tag{24}$$

$$\gamma_\lambda = 2.13 \left(\frac{\nu\varepsilon}{k^2}\right)^{1/4} \tag{25}$$

The mass transport between the fine structures and the surroundings is expressed by

$$\dot{m} = 23.6 \left(\frac{\nu\varepsilon}{k^2}\right)^{1/4} \frac{\varepsilon}{k} = 11.08 \, \gamma_\lambda \frac{\varepsilon}{k} \tag{26}$$

and the reactants to products conversion rate by

$$\tilde{R}_{fu} = \bar{\varrho}\tilde{\omega}_{fu} = \dot{m} \frac{\chi}{1-\chi\gamma^*} \frac{\tilde{\varrho Y}_{min}}{\gamma_\lambda} \tag{27}$$

where $\tilde{Y}_{min}$ is the limiting reactant

$$\tilde{Y}_{min} = \min (\tilde{Y}_{fu}, \tilde{Y}_{O_2}/\nu_{fu}) \quad (28)$$

and χ is the fraction of fine structures sufficiently heated to react given by

$$\chi = \frac{1}{\gamma_\lambda} \frac{\tilde{Y}_{pr}/(1+\nu_{fu})}{\tilde{Y}_{pr}/(1+\nu_{fu})+\tilde{Y}_{min}} \quad (29)$$

Physical restrictions call for the following limitations in the preceding expressions

$$\chi \leq 1 \quad (30)$$

and

$$\frac{\tilde{Y}_{min}}{\gamma_\lambda} \leq \tilde{Y}_{fu,stoich} \quad (31)$$

According to the above concept the reaction rate in most of the central zone of a propagating flame is expressed in conformity with

$$R_{fu} = \dot{m}\, \bar{\varrho}\tilde{Y}_{fu,stoich} \quad (32)$$

while the reaction rate of the leading edge tends towards

$$R_{fu} = \frac{\dot{m}}{\gamma_\lambda} \bar{\varrho}\tilde{Y}_{pr}/(1+r_{fu}) \quad (33)$$

and reaction rate of the trailing edge approaches

$$R_{fu} = \frac{\dot{m}}{\gamma_\lambda} \bar{\varrho}\tilde{Y}_{min} \quad (34)$$

3 Numerical Procedure

The Simplified-Arbitrary-Lagrangian-Eulerian computer program SALE[14] extended to include a general diffusion term with variable viscosity, a user defined number of general purpose transport equations, methods of acceleration of convergence, calculation of thermodynamic properties and models of turbulence and combustion is used.

4 Calculations and Discussion of The Results

In order to test and validate the numerical model with closure models, the calculated results are compared with experimental data in engine and engine-like conditions.

At the present stage it has been desired to do this investigations under condititons of unsophisticated geometries and flow fields, to minimize the number of controlling parameters. This has been done since the engine operating cycle even in its simplest form is exceedingly complex. Consequently all calculations are done with a flat headed, pancake piston cylinder geometry and without additional squish or swirl effects. The most of available experimental data is also limited to simple piston/cylinder configurations.

The comparisons are divided into two parts. In the first part, which is not reported here, calculated pure hydrodynamic results are compared with measured results of a non firing transparent axis symmetric piston-cylinder model engine, used in the experiments of Morse, Whitelaw and Yianneskis [15]. In the second part the calculated combustion rate is verified by comparing the calculated mass fraction burnt with data for an axis symmetric homogeneous charge spark ignition engine given by Groff, Alkidas and Meyers [16]. The main specifications of the engine are given in Table I. Results from the pure hydrodynamic calculations and qualitative and quantitative comparisons between calculated and measured results are reported by Grimsmo and Magnussen [17].

The calculations with combustion are performed with four different variations of the turbulence model. In Case I all the extension terms of the k-ε-model are activated, that means the turbulence model includes both dilatation effect terms and the pressure-density effect term, the constant C_3 is set equal to -0.33 and C_4 $(1/\sigma_t)$ is set equal to 1.25. Case II and III both include dilatation effect terms but omit the pressure/density effect term, in Case II C_3 is set equal to -0.33 and in Case III C_3 is set equal to 1, this is done to test the effect of the most frequently used values of this constant which appear with different values [18,19] in the literature. In Case IV both extension terms are inactivated.

Figures 1 and 2 show results from the four cases (I to IV) of pure hydrodynamic calculations. The turbulent velocity scale and the length scale, at a point near the edge of the suction jet, are plotted versus the crank angle. Case I and II coincide since there are almost no pressure gradients present. The highest turbulence intensity is predicted in Case II with C_3 equal 1.0, but in this case the length scales become very large. If they had not been limited by the boundary restriction they would probably grow beyond the size of the clearance hight (here 0.0126 m). As expected, Case I predicts a higher turbulent intensity during the compression stroke than Case II due to its dilatation term.

Figure 3 shows results from three cases (I,II and IV) of combustion calculations. The measured and calculated mass fraction burnt is plotted versus the crank angle. Case I and II again coincide and indicate the minor significance of the pressure-density effect term. Case I, with its dilatation effect term shows a better agreement with the measurements than Case IV.

Figures 4-8 show results from Case IV of the combustion calculation. All these figures show values at a cross-section located midway

between the piston and the cylinder top. Figure 4 shows how the mass fraction burnt propagates from the cylinder centre awards the cylinder wall by means of a sequence of plots at different crank angles. Figure 5 shows the distribution of the reaction rate at a crank angle equal 351 ATDC and illustrates the flame zone and position at this angle. The corresponding results for the production terms of the extended model are plotted in Fig. 6. They show how the dilatation term produces turbulent energy in front of the flame, while the pressure-density term produces turbulence more or less inside the flame zone. Figures 7 and 8 show the progression of the terms.

Figure 9 a)-e) show a sequence of calculated results of the flame development with the fully extended model, each spaced in time by one millisecond. In the figures the velocity vectors and isolines for fractional mass conversion are shown. The movement of these lines defines the propagation of the flame. The corresponding mass of fuel conversion is shown in Fig. 10.

Ignition is numerically initiated at the centre of the cylinder right under the inlet valve and from here the flame front starts forming, see Fig. 9. At this stage the turbulence is controlled by the decay rate of a relatively small rest of intake generated turbulence and some turbulence generated due to compression by the piston. The leading edge enters into the unburnt mixture, the flame propagation begins and the expansion of the combusting gases starts pushing the unburnt gas ahead of the flame front. A substantial portion of the chamber is filled with burnt gas before a noticeable fraction of the total mass is burnt, see also Fig. 10.

The initial flame is spherical and remains spherical until the flame reaches the piston top. From this point the flame surface can not expand freely any longer but continues across the combustion chamber with the clearance height as a limiting factor on the front area which engulf new unburnt mixture. This situation elucidate some of the spark location's effect on the ratio between the volume engulfed and the area engulfing, which is known to influence on the burning time.

The observed total flame propagation in the figures is the sum of the transport velocity related to the expansion of fluid and the burning velocity related to the reaction rate.

The expansion velocity increases in the beginning of the combustion period and after a while it forms the overall velocity facing outward. Now the turbulence is mainly controlled by the generated shear flow, the compression due to combustion and by compression due to piston motion.

When the flame has left its initial position and burnt gas is left behind the flame front, a reverse flow is generated in the opposite direction of the main expansion flow. This effect seems to stretch the flame zone in both directions.

Behind the leading edge, a region of gradual combustion remains. This region forms the turbulent flame thickness and its width is in the same order as the clearance height between the piston and the cylinder top. It should be emphasized that the flame region does

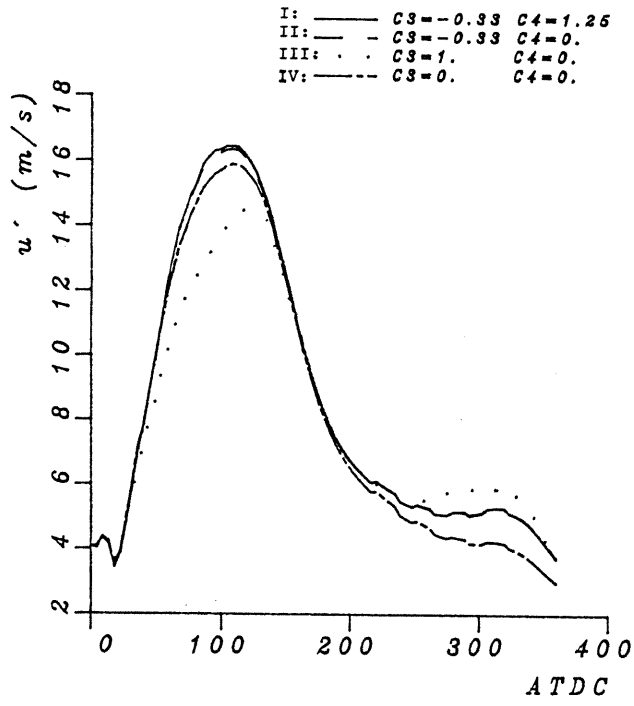

Fig. 1. Turbulence velocity scale versus crank angle.

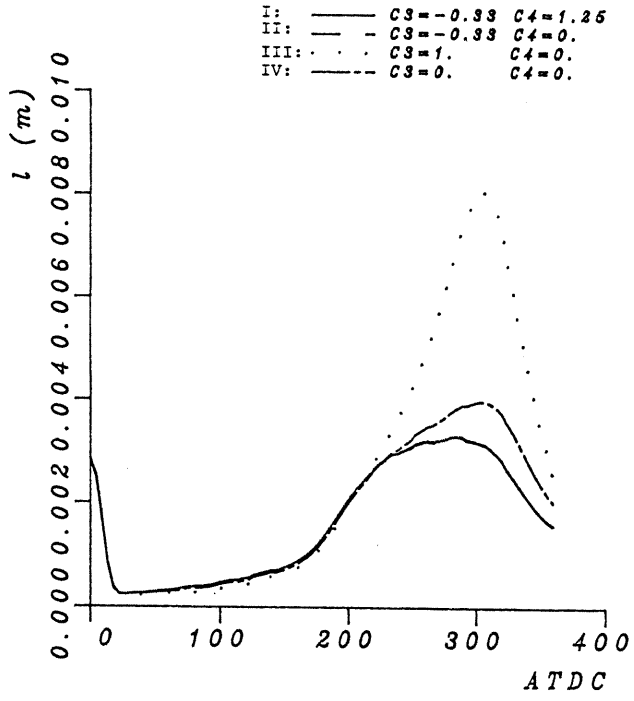

Fig. 2. Turbulence length scale versus crank angle.

not represent an instant picture of the flame, but represents the time average statistically possible occurrence or the prevalence of existence the flame. The overall turbulent flame thickness is, due to large scale turbulent fluctuations, expected to be considerably larger than the corresponding instantaneous flame thickness.

When the leading edge of the flame gets close to the cylinder wall zone, the flow changes main direction towards the centre of the cylinder. This is a consequence of conservation of mass. The fraction of burnt gas is still relatively small due to a mass versus volume effect which is recognized by the higher density of the unburnt gases.

Finally propagation slows down, but the combustion continues within the flame itself. Since the volume to be burnt increases with the distance from the cylinder centre and because of the mentioned higher density, a relatively large fraction of the fuel will burn at this final stage.

These results correspond qualitatively well with the observations and measurements of Gatowski, Heywood and Deleplace[20], and the same qualitative picture can be found in the works by Namazian et al. [21] and Inuma and Iba [22].

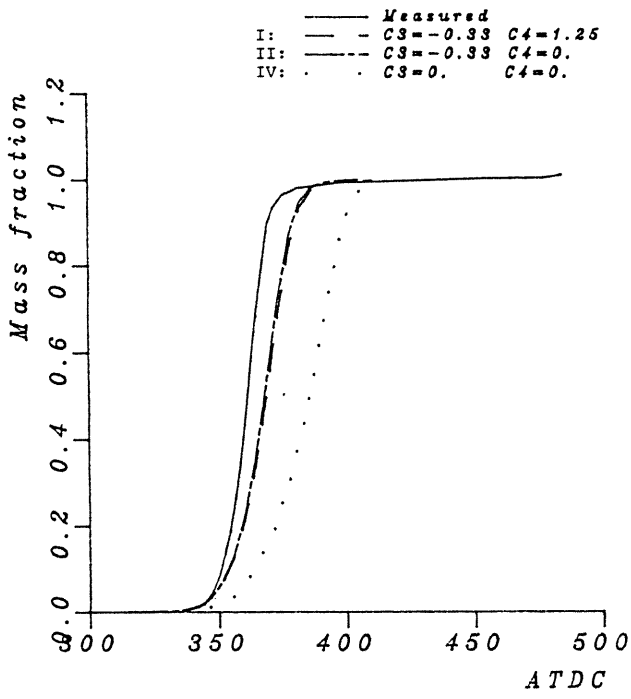

Fig. 3. Calculated and measured mass burnt fraction versus crank angle.

	Engine specifications
Bore	0.1047 m
Stroke	0.0953 m
Clearance	0.0126 m
Compression ratio	8.56
Chamber shape	disk
RPM	1500 rpm
Volumetric efficiency	0.6
Fuel	Propane
Equivalent ratio	0.8969
Sparkplug location	central

Table I. Overall engine specifications of the experiments [16].

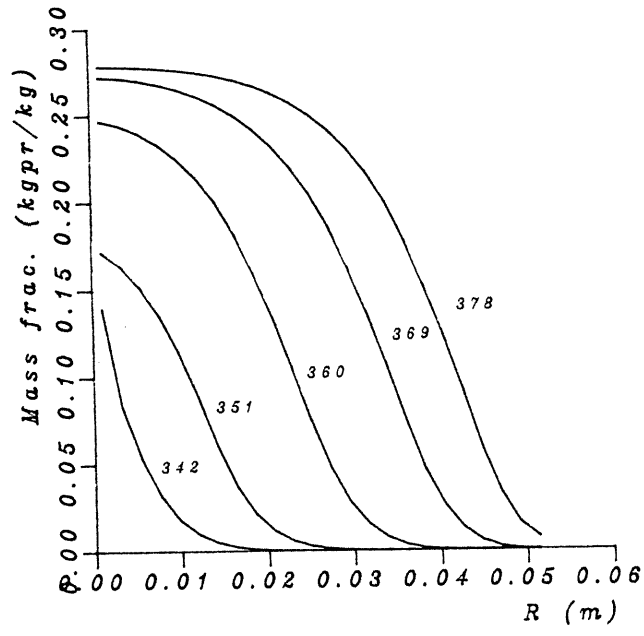

Fig. 4. Mass fraction of products at a cross-section located midway between piston and cylinder top at different crank angles.

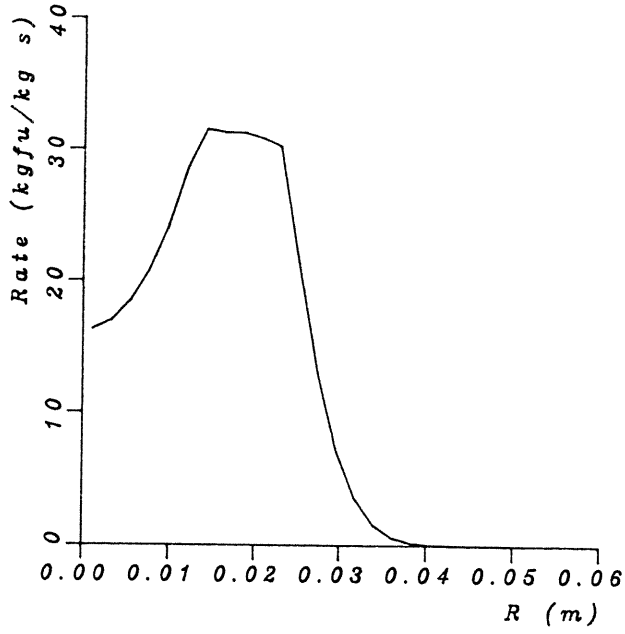

Fig. 5. Mass fraction of products at a cross-section located midway between piston and cylinder top at 351 ATDC.

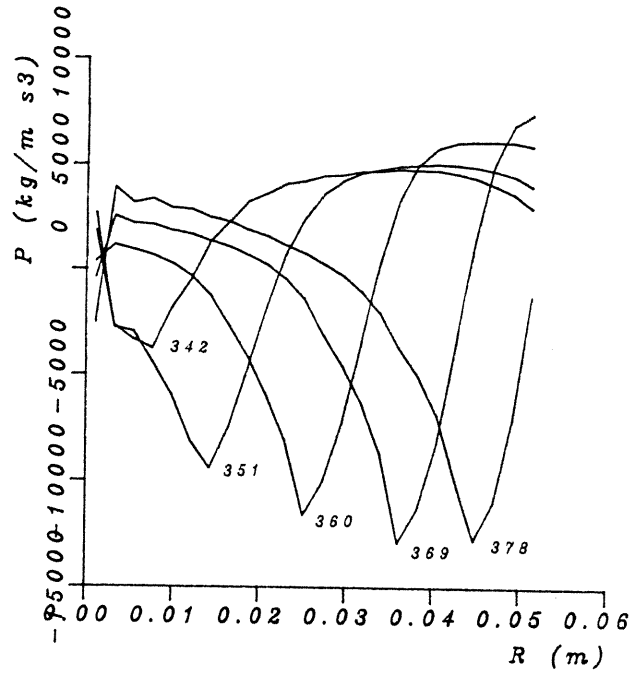

Fig. 7. Production of turbulent kinetic energy due to dilatation at a cross-section located midway between piston and cylinder top at different crank angles.

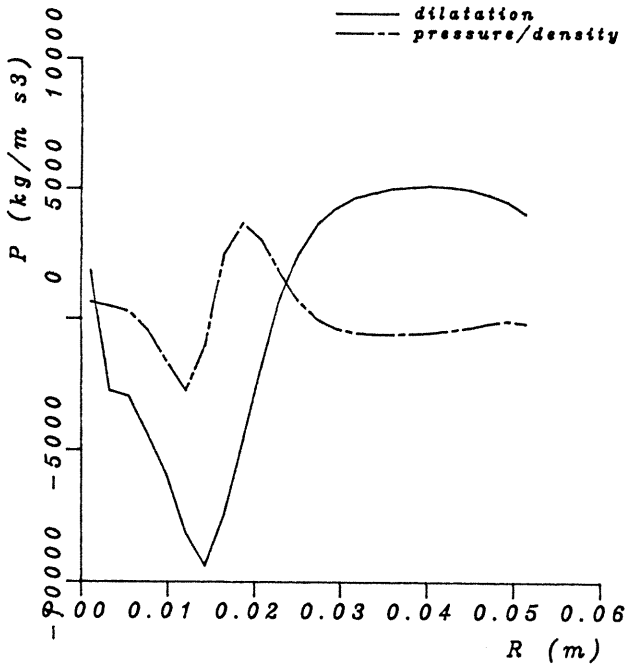

Fig. 6. The two new production terms in the k-equation at a cross-section located midway between piston and cylinder top at 351 ATDC.

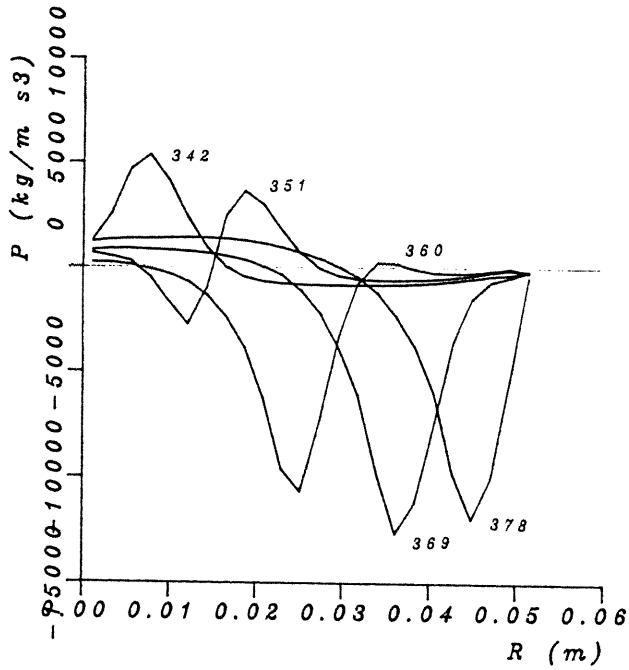

Fig. 8. Production of turbulence kinetic energy due to pressure-density effects at a cross section located midway between piston and cylinder top at different crank angles.

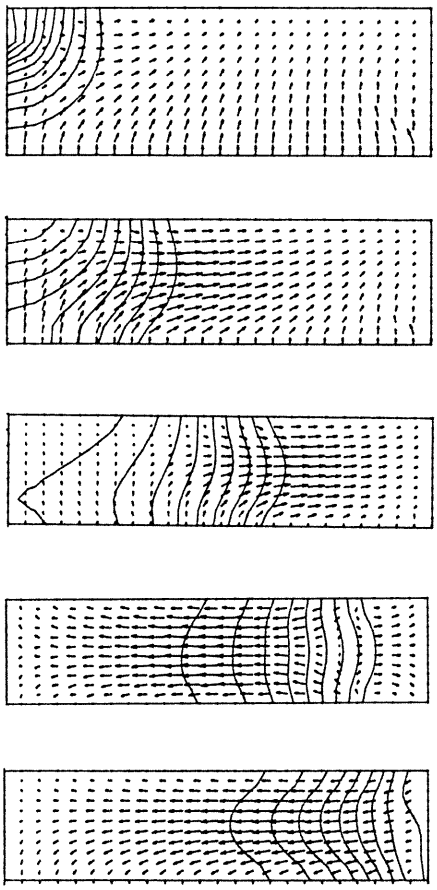

Fig. 9. A-E gives a sequence of results for the flame development, spaced in time by a millisecond. Shown in the figures are the isolines for the fractional mass conversion and the velocity vectors.

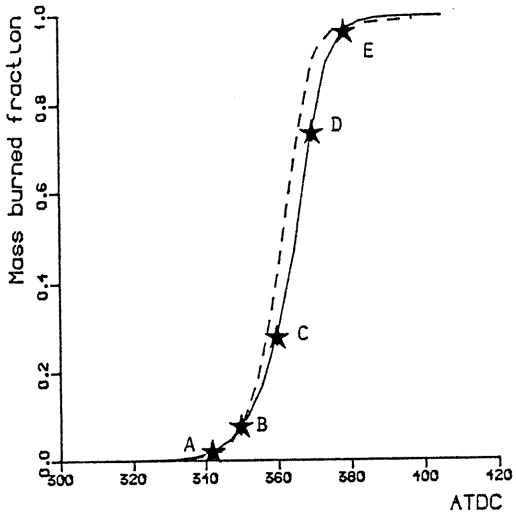

Fig. 10. Mass burnt fraction versus crank angle. The markers A-E corresponds to Fig. 9. Measured data [16] is shown by the dashed line.

5 Conclusions

The comparisons between the calculated results and data from experiments found in the literature show that it is possible by means of fundamental equations and existing phenomenological theory to calculate with reasonable accuracy the spatial and temporal distribution of physical properties inside the enclosed volume of an engine cylinder. These are difficult to obtain by costly and time consuming experiments and can not be found by simple analytical theory.

However, the application of research of this kind is relatively new and there are problems that remain to be solved. Most distinct is the limited knowledge about the turbulent structure of the flow near the walls. Also, the lack of knowledge about turbulent parameters at the inflow boundaries causes uncertainties in the calculated results.

The possibility of including finite rate chemistry has been kept in mind during the present work and in the future the developed numerical tool may serve as a basis for simulation of ignition, extinction and knock effects.

Nomenclature:

C,D	model constants
c_v	specific heat constant
ΔE	internal heat of combustion
k	turbulent kinetic energy
l	length scale of turbulence
L	characteristic length scale
m	mass
P_k	turbulence production term
p	pressure
q	heat transport rate
R	reaction rate
r_{fu}	stoichiometric oxygen requirement
S_φ	general source term
t	time
u	velocity
x	spatial coordinate
Y	mass fraction
y	distance from wall

Greeks

δ_{ij}	Kronecker delta
ε	dissipation rate of turbulence
φ	general value
Γ	diffusivity
γ	mass fraction occupied by fine structures
μ	viscosity
ω	source of species
χ	fraction of fine structure that react
ϱ	density
σ	turbulent Prandtl/Schmidt number

Sub- and superscripts

i,j,l	directional indexes
-	ordinary time average
~	mass weighted time average
"	mass weighted turbulent fluctuation
fu	fuel
fuel	fuel
O_2	oxygen
prod	products
t	turbulent
*	fine structure
λ	fine structure region
nw	near the wall
w	at the wall

REFERENCES

1. Gupta H.C., Steinberger R.L. and Bracco F.V.: Comb. Sci. and Tech., Vol 22, pp.27-61, 1980.
2. Ahmadi-Befrui B.,Gosman A.D.,Lockwood F.C. and Watkins A.P.: SAE 810151, 1981.
3. Gosman A.D. and Hervey P.S.: SAE 820036, 1982.
4. Brandstätter W. and Johns R.J.R.: C58/85 IMechE, 1983.
5. Butler T.D., Cloutman L.D., Dukowicz J.K. and Ramshaw J.D.: Prog. Energy. Combust. Sci. Vol. 7, pp.293-315, 1981.
6. Syed S.A. and Bracco F.V.: SAE 790247, 1979.
7. Grasso F. and Bracco F.V.: Comb. Sci. and Tech., Vol 28, pp.185-210, 1981.
8. Markatos N.C. and Mukerjee T.: IMACS, North-Holland, 1981.
9. Przekwas A.: "Modeling of Fluid Flow Heat Transfer and Flame Propagation in Reciprocating Engines" Paper presented at ASME - winter annual meeting, New Orleans, 1984.
10. Magnussen B.F.: "Modeling off NOx and Soot Formation by The Eddy Dissipation Concept", Paper presented at the International Flame research Foundation, 1st Topic Oriented Technical Meeting, Amsterdam, 1989.
11. Launder B.E., and Spalding D.B.: "Mathematical Models of Turbulence", Academic Press, 1972.
12. Chomiak J. "Turbulent Reacting Flows", Lecture series at the Norwegian Institute of Technology, spring 1985.
13. Mattavi J.N. and Amann C.A.: Combustion Modeling i Reciprocating Engines, p.69, Plenum Press, 1980.
14. Amsden A.A., Ruppel H.M. and Hirt C.W.: "SALE", Los Alamos Scientific Laboratory report, LA-8095, 1980.
15. Morse A.P., Whitelaw J.H., and Yianneskis M.: "Turbulent Flow Measurements by Laser-Doppler Anemometry in a motored Reciprocating Engine", Imperical College of Science and Technology, Department of Mechanical Engineering, Fluid Section, London SW7 2BX, FS/78/24, 1978.
16. Groff E.G., Alkidas A.C. and Meyers J. P.: "Combustion Data for an Axis Symmetric Homogeneous-Charge Spark-Ignition Engine", Engine Research Department, General Motors Research Laboratories, 1981.
17. Grimsmo B. and Magnussen B. F.: "Numerical Simulation of Flow and Combustion in an Homogeneous Charge Spark Ignition Engine, Comparison with Experimental data" Paper presented at the Task Leader Conference, IEA, Ottawa, Canada, 1987
18. Morel T. and Mansour N.N.: SAE 820040, 1982.
19. Ahmadi-Befrui B.: ASME 87-FE-11, The Energy-Sources Technology Conference and Exhibition, Dallas, 1987.
20. Gatowski J.A., Heywood J.B. and Deleplace C.: Comb. and Flame Vol.56: 71-81, 1984.
21. Namazian M., Hansen S., Lyford-Pike E., Sanchez-Barsse J., Heywood J. and Rife J.: SAE 800044, 1980.
22. Inuma K. and Iba Y.: JARI technical memorandum no. 15, 1973.